Journal of Power Sources 195 (2010) 3425–3430

Contents lists available at ScienceDirect

Journal of Power Sources

journal homepage: www.elsevier.com/locate/jpowsour

High temperature polymer electrolyte membrane fuel cell performance of Pt_xCo_y/C cathodes

Ch. Venkateswara Rao, Javier Parrondo, Sundara L. Ghatty, B. Rambabu*

Solid State Ionics and Surface Science Laboratory, Department of Physics, Southern University and A&M College, Baton Rouge, LA 70813, USA

ARTICLE INFO

Article history:
Received 7 October 2009
Received in revised form 4 December 2009
Accepted 7 December 2009
Available online 16 December 2009

Keywords:
High temperature PEMFCs
Pt–Co alloys
Polybenzimidazole
Cathode
Borohydride reduction method

ABSTRACT

Carbon-supported Pt–Co alloy nanoparticles of varying Pt:Co atomic ratios of 1:1, 2:1, 3:1 and 4:1 are prepared, characterized and tested in high temperature PEM fuel cell intend to reduce the Pt loading. These electrocatalysts are prepared by borohydride reduction method in the presence of citric acid as stabilizing agent. Face-centered cubic structure of Pt is evident from XRD. The positive shift of Pt diffraction peaks with increasing cobalt content in the Pt_xCo_y/C catalysts indicated the solubility of Co in Pt lattice. The average crystallite size is found to be 6 nm in all the prepared catalysts. The electrochemical active surface area (EAS) of the catalysts from CO-stripping voltammetry is calculated to be 65.2, 51.4, 47.7, 41.5 and 38.3 $m^2\ g^{-1}$ Pt for Pt/C, Pt–Co(4:1)/C, Pt–Co(3:1)/C, Pt–Co(2:1)/C and Pt–Co(1:1)/C, respectively. These catalysts are used as cathode in the fabrication of polybenzimidazole-based membrane electrode assembly (MEA) and the polarization curves are recorded at 160 and 180 °C. The results indicate the good performance of Pt–Co alloys than that of Pt under the PEM fuel cell conditions. Among the investigated electrocatalysts, Pt–Co(1:1)/C and Pt–Co(2:1)/C exhibited good fuel cell performance. Durability tests also indicated the good stability of Pt–Co(1:1)/C and Pt–Co(2:1)/C compared to Pt/C.

1. Introduction

Polymer electrolyte membrane fuel cells (PEMFCs) attract great interest as power sources for zero-emission vehicles and stationary applications due to their high efficiency and low-air pollution when compared with internal combustion engines. PEMFCs operated at high temperatures (≥160 °C) offer several advantages than the low temperatures (≤100 °C) in terms of fuel cell efficiency, performance, kinetics of electrodic reactions, water management and tolerance to contaminants [1]. Even then the performance and efficiency are not sufficient to meet the desirable characteristics and also for commercialization. One of the issues mitigating the performance is the sluggish kinetics of oxygen reduction reaction (ORR) at cathode side [2]. Carbon-supported Pt is the successful cathode at the present stage, but still the ORR kinetics on Pt should be improved and Pt loading should be decreased. It is certainly true that the move toward Pt alloys as the catalyst for ORR is necessary, but many issues still need to be resolved [3,4].

In terms of efficient cathode materials for ORR, there has been significant research focused on platinum alloys to lower the overpotential, increase the oxygen reduction activity and reduce the amount of Pt. Pt has been alloyed with a variety of elements including V, Cr, Ti, Mn, Fe, Co, Ni, W, Mo, Ir, Pd, Zn. An enhancement in activity (1.5–5 times) for ORR on the alloy catalysts in comparison to pure Pt has been reported using potentiodynamic RRDE measurements [5–22]. It was also reported that the overpotential for the ORR on Pt alloys is 20–40 mV less compared to Pt. Among the various Pt bimetallic alloys, Pt–Co appears to be good. Usually, the carbon-supported Pt alloy catalysts are prepared by the impregnation of the second metal on Pt/C and then alloying at temperatures above 973 K under reducing Ar–H_2 gas atmosphere [23]. But the heat-treatment at high temperatures gives rise to an undesired particle growth of the alloy; induce the sintering of particles and causes the loss of surface area, which results in the decrease in specific activity for ORR.

The fuel cell performance was found to depend significantly on the sub-surface composition. Various authors reported that the bimetallic Pt–Co in 1:1 or 2:1 or 3:1 as optimum for good performance depending on the experimental conditions. Mukerjee and Srinivasan [5] reported bulk Pt–Co alloys with atomic ratio 1:1 exhibited good ORR activity. According to Xiong et al. [9], who prepared various carbon-supported Pt–Co electrocatalysts by a low temperature reduction procedure with sodium formate, reported that the Pt–Co electrocatalyst showed the best performance with the maximum catalytic activity and minimum polarization at a Pt:Co atomic ratio of around 1:7. Toda et al. [7] investigated the electrocatalytic ORR activity of Pt alloys with Co formed by sputtering, and observed maximum activity at *ca.* 40, 50 and 30% content

* Corresponding author. Tel.: +1 225 771 2493/4130; fax: +1 225 771 2310.
E-mail address: rambabu@cox.net (B. Rambabu).

0378-7753/$ – see front matter © 2009 Elsevier B.V. All rights reserved.
doi:10.1016/j.jpowsour.2009.12.022

of Co respectively. They also observed an increase in kinetic current densities by which 10 times larger than that of pure Pt. Kinetic analysis of the data in comparison to pure Pt, revealed an activity enhancement of a factor of 2–3 for the 50 at.% Co-catalyst [8]. Huang et al. [18] prepared carbon-supported Pt–Co alloy catalysts with different Pt/Co atomic ratios, 1:1, 2:1, 3:1, 4:1 and 5:1 by the carbonyl complex route followed by H_2 reduction in the temperature range of 423–573 K and reported the maximum activity with a Pt/Co atomic ratio of 2:1. Grinberg et al. [19] prepared carbon-supported Pt–Co alloys in 1:1 atomic ratio by the thermal decomposition of organometallic complexes of Pt and Co and found good ORR activity than Pt alone. The inconsistency is due to the variation of geometric factors (degree of alloying and Pt–Pt interatomic distance) and electronic factors (Pt d-band vacancies) resulting from the preparation methods and heat-treatments.

In the present study, carbon-supported Pt_xCo_y (x = 1, 2, 3 and 4; y = 1) alloy nanoparticles are prepared by wet chemical method and characterized by XRD, SEM, and EDX. The electrochemical performance of the Pt_xCo_y/C as cathode in PEMFC operated at ≥160 °C is investigated and compared with that of Pt/C.

2. Experimental

2.1. Materials

Hexachloroplatinic acid, cobalt chloride, citric acid (98%), sodium borohydride (98%), 3, 3′-diaminobenzidine (99%), N,N′-dimethylacetamide (99.5%), lithium chloride (99+%) and polyphosphoric acid (115%) were purchased from Sigma Aldrich and used as received. Isophthalic acid was purchased from Alfa Aesar (99%) and purified by recrystallization in ethanol prior to use. Vulcan XC72R carbon black (Cabot, USA) was used as the supporting material of the Pt and Pt–Co alloy nanoparticles.

2.2. Preparation of Pt_xCo_y/C electrocatalysts by borohydride reduction method

In a typical synthesis, aqueous solutions of hexachloroplatinic acid ($H_2PtCl_6{\cdot}6H_2O$) and cobalt chloride ($CoCl_2{\cdot}6H_2O$) are mixed with citric acid and stirred for 30 min to form complexes. pH of the solution is found to be around 5. To the yellow color solution, 0.3 g of Vulcan XC-72R carbon is added and stirred for 1 h. Then 0.3 g of $NaBH_4$ dissolved in 50 mL de-ionized water (freshly prepared) is added dropwise to the above suspension and continuously stirred for 5 h. After the addition of aqueous $NaBH_4$, yellow color solution turns colorless due to the reduction of metal ions to metal particles. Finally, the suspension is filtered, washed copiously with de-ionized water and dried at 353 K for 2 h under vacuum. Carbon-supported Pt–Co alloy nanoparticles of varying Pt:Co atomic ratios of 1:1, 2:1, 3:1 and 4:1 are prepared. For comparison, carbon-supported Pt is also prepared. The nominal metal loading on the carbon is 40 wt.% in all the catalysts.

2.3. Synthesis of m-polybenzimidazole and fabrication of PBI membranes

m-Polybenzimidazole (m-PBI) polymer was synthesized following the procedure described by Xiao et al. [24]. In a typical synthesis, 3.7135 g of isophthalic acid (22.35 mmol) and 4.7896 g of 3, 3′-diaminobenzidine (22.35 mmol) were added to a three-neck reaction flask in an argon filled glovebox, followed by 91.5 g of polyphosphoric acid. The reaction mixture was stirred using a mechanical overhead stirrer and purged with a slow stream of nitrogen. The reaction temperature was maintained at 190–220 °C for 16–24 h. Polybenzimidazole solution (5 wt.% PBI) used in the preparation of catalyst ink was prepared by heating PBI and LiCl (1.5 wt.% LiCl) in dimethylacetamide at 250 °C during 6 h. Inherent viscosity (IV) of the polymer was measured at a polymer concentration of 2 kg m^{-3} in concentrated sulfuric acid (96 wt.%) at room temperature using an Ubbelohde viscometer.

The membranes used in fuel cell experiments were prepared by casting the PPA polymer solution onto glass plates using an adjustable film applicator (GARDCO MICROM II, Paul N. Gardner Company). The gate clearance was fixed in 0.006 in. to obtain after hydrolysis membranes of approximately 100 μm. Since polyphosphoric acid (PPA) is extremely hygroscopic, moisture is absorbed from the atmosphere and PPA is being hydrolyzed to phosphoric acid producing a gel that contains high amounts of phosphoric acid. The concentration of phosphoric acid was estimated weighing a membrane sample before and after removing phosphoric acid by washing with ammonium hydroxide. The details of the chemistry involved in gel formation can be encountered in Mader et al. [25].

2.4. Characterization techniques

XRD measurements were performed on a Rigaku D/max-RA X-ray diffractometer using a CuKα source (λ = 1.5406 Å) operated at 40 kV at a scan rate of 0.025° per second over the 2θ range of 10–90°. A scanning electron microscope (JEOL JSM-840) equipped with EDX was used to observe the surface morphology and elemental composition of the prepared catalysts.

2.5. Electrochemical measurements

In order to calculate electroactive surface area (EAS) of the prepared electrocatalysts, CO-stripping voltammograms were recorded at room temperature using a three electrode, one-compartment electrochemical glass cell assembled with glassy carbon (GC) disk as the working electrode, Ag/AgCl, 3.5 M KCl (+0.205 V vs. NHE) as the reference and Pt foil as the counter electrodes, respectively in a potentiostat (Princeton Applied Research Potentiostat/Galvanostat model 273A). The working electrode is fabricated by dispersing 5 mg of the catalyst in 5 mL of isopropanol by ultrasonication for 20 min. An aliquot of 20 μL catalyst suspension was pipetted onto the glassy carbon (GC) substrate. After evaporation of the isopropanol in an argon stream, the deposited catalyst was covered with 10 μL of a diluted Nafion® solution and dried at room temperature. Current densities are normalized to the geometric area of the glassy carbon substrate (0.07 cm^2). For CO-stripping voltammetry measurements, pure CO was bubbled into the 0.5 M $HClO_4$ electrolyte for 30 s and then its adsorption on the electrode was driven under potential control at 0.2 V vs. NHE for 1 min. After fabrication, the electrodes are immersed in the electrolyte and the voltammograms were recorded in the potential region of +0.5 and +1.1 V vs. NHE to electro-oxidize the irreversibly adsorbed CO and the subsequently voltammograms were recorded in order to verify the completeness of the CO oxidation.

2.6. Membrane electrode assembly (MEA) fabrication and high temperature PEMFC testing

MEAs with an active area of 3.24 cm^2 were assembled by placing two gas diffusion electrodes (GDEs) at each side of the PBI membrane. The MEA was assembled in a 5 cm^2 single cell PEMFC with single serpentine flow fields (Fuel Cell Technologies, Inc.), using sub-gaskets to avoid direct pressure of the gaskets over the membrane and hence protecting the membrane from excessive pressure and stress during heating. The sub-gaskets had a thickness of 25 μm and the gaskets 395 μm. The pinch, defined as the difference between the MEA and the gaskets thickness was 75 μm.

Gas diffusion electrodes were prepared by painting with an air-brush the microporous area of a gas diffusion layer (GDL Sigracet

GDL 10BB, 420 μm, SGL Carbon Group). Catalyst ink consisted of home-made carbon-supported catalyst (0.2 g) to which DMAc (7.5 g) and 5 wt.% PBI solution (0.211 g) were added. The ink slurry was stirred overnight to break up the catalyst powder in order to get a homogenous ink. During the painting, the gas diffusion layer was kept near an IR lamp to dry the ink between each application. The metal loading of each electrode was measured by the difference in weight before and after painting and was kept in $0.50 \pm 0.05\ mg\ cm^{-2}$. The anode was fabricated using commercial Pt/C catalyst (platinum nominally 40% on carbon black, Alfa Aesar) with a loading of $0.5\ mg\ Pt\ cm^{-2}$.

The performance was evaluated after conditioning for 24 h at $200\ mA\ cm^{-2}$. The polarization curves were recorded at atmospheric pressure using dry oxygen and hydrogen at 160 and 180 °C. Stoichiometric ratios of 1.2 for hydrogen and 2 for oxygen, with minimum flows of $0.1\ L\ min^{-1}$ (hydrogen) and $0.2\ L\ min^{-1}$ (oxygen) were employed in the experiments. A Compact Fuel Cell Test System model 850e (Scribner Associates, Inc.) controlled using FuelCell® 3.9c software (Scribner Associates, Inc.) was used. Cell resistance was measured at each operating condition by using the current-interrupt and high-frequency impedance (1000 Hz) techniques build into the fuel cell test station.

The electrode ionic resistance was evaluated using impedance spectroscopy (Princeton Applied Research Potentiostat/Galvanostat model 273A). The electrode resistance was calculated by measuring the horizontal distance of the 45° branch in the impedance spectra ($R_e/3$) [26,27]. AC impedance spectra were recorded in H_2/N_2 mode using the fuel cell cathode as working electrode and the anode as counter electrode by applying an AC signal of 15 mV amplitude superimposed to a DC signal of 0.3 V in the frequency range 50 kHz–0.1 Hz. Impedance measurements were taken after stabilization of the system for at least 15 min.

3. Results and discussion

3.1. XRD analysis

Powder XRD patterns of the carbon-supported Pt and Pt_xCo_y ($x = 1$, 2, 3 and 4; $y = 1$) alloy electrocatalysts recorded in the 2θ range of 10–90° are shown in Fig. 1. As can be seen, all the catalysts exhibited five characteristic diffraction peaks at 2θ values around 40°, 47°, 68°, 82° and 87° corresponding to the (1 1 1), (2 0 0), (2 2 0), (3 1 1) and (2 2 2) planes of face-centered cubic (fcc) structure of Pt (JCPDS No. 87-0640). The broad peak observed at around $2\theta = 25°$ is due to the hexagonal structure of carbon support. No peaks corresponding to the Co or its oxides were observed. The broad diffraction peaks suggests the nanocrystalline Pt and/or Pt–Co species on carbon support. The average crystallite sizes of Pt or Pt–Co alloys supported on carbon are calculated from line broadening of the (2 2 0) diffraction peak (Gaussian–Lorentzian peak) according to Scherrer's equation: $L = 0.9\lambda/\beta_{1/2} \cos\theta$ where λ is the wavelength of the X-ray (0.15406 nm), θ is the angle at the position of the peak maximum and $\beta_{1/2}$ is the width (in radians) of the diffraction peak at half height and the values are given in Table 1. The average crystallite size of 6 nm is observed in all the prepared catalysts due to the identical conditions maintained during the preparation procedure. In the case of Pt_xCo_y/C catalysts, diffraction peaks are shifted to higher 2θ values with respect to the corresponding peaks in the Pt/C catalyst. Also the extent of shifting increases with the content of cobalt in Pt_xCo_y/C catalysts. The lattice parameter (a) and Pt–Pt interatomic distance calculated from the θ and $\beta_{1/2}$ of diffraction peaks is given in Table 1. The gradual decrease of lattice parameter with cobalt content in the Pt_xCo_y/C catalysts (obeying Vegard's law) indicating the solubility of Co in face-centred cubic Pt lattice. The extent of shift also suggests that the interatomic distance of Pt is decreased due to the substitution of cobalt. It is known that oxygen is adsorbed on Pt surface by dual site mode; therefore the Pt–Pt nearest-neighbor distance plays the key role to determine the adsorption behavior. Jalan and Taylor [22] have studied the effect of Pt–Pt nearest-neighbor distance and oxygen reduction activity of various platinum alloys. They claimed that the short Pt–Pt nearest-neighbor distance in alloys compared to that of the pure Pt causes the facile reduction of oxygen. So the contraction of Pt lattice observed in the case of as-prepared catalysts may be favourable for dissociation of oxygen and enhance the kinetics thereby fuel cell performance.

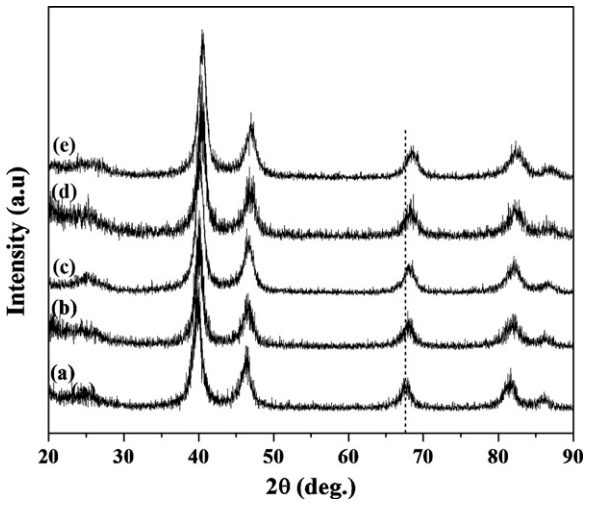

Fig. 1. Powder XRD pattern of carbon-supported Pt and Pt–Co catalysts: (a) Pt/C, (b) Pt–Co(4:1)/C, (c) Pt–Co(3:1)/C, (d) Pt–Co(2:1)/C and (e) Pt–Co(1:1)/C.

3.2. SEM and EDX analyses

The scanning electron microscopic (SEM) images of carbon-supported Pt and Pt_xCo_y are shown in Fig. 2. Good spatial distribution of metal particles on carbon support was observed. The elemental composition (Pt:Co) calculated from the EDX spectra of the carbon-supported Pt and Pt_xCo_y alloy catalysts is given in Table 1. It was observed that the average compositions were nearly in agreement with those of the initial metal salt solutions.

Table 1
Lattice parameter, Pt–Pt interatomic distance, crystallite size, EDX composition and electrochemical surface area of the catalysts.

Catalyst	Lattice parameter (nm)	Pt–Pt interatomic distance (nm)	Crystallite size (nm)	EDX composition (wt.%) Pt:Co	Electrochemical surface area ($m^2\ g^{-1}$ Pt)
Pt/C	0.3919	0.2771	6.1	100:-	65.2
Pt–Co(4:1)/C	0.3908	0.2764	6.0	92.8:7.2	51.4
Pt–Co(3:1)/C	0.3884	0.2747	6.2	90.7:9.3	47.7
Pt–Co(2:1)/C	0.3868	0.2736	6.1	86.8:13.2	41.5
Pt–Co(1:1)/C	0.3814	0.2697	6.1	76.7:23.3	38.3

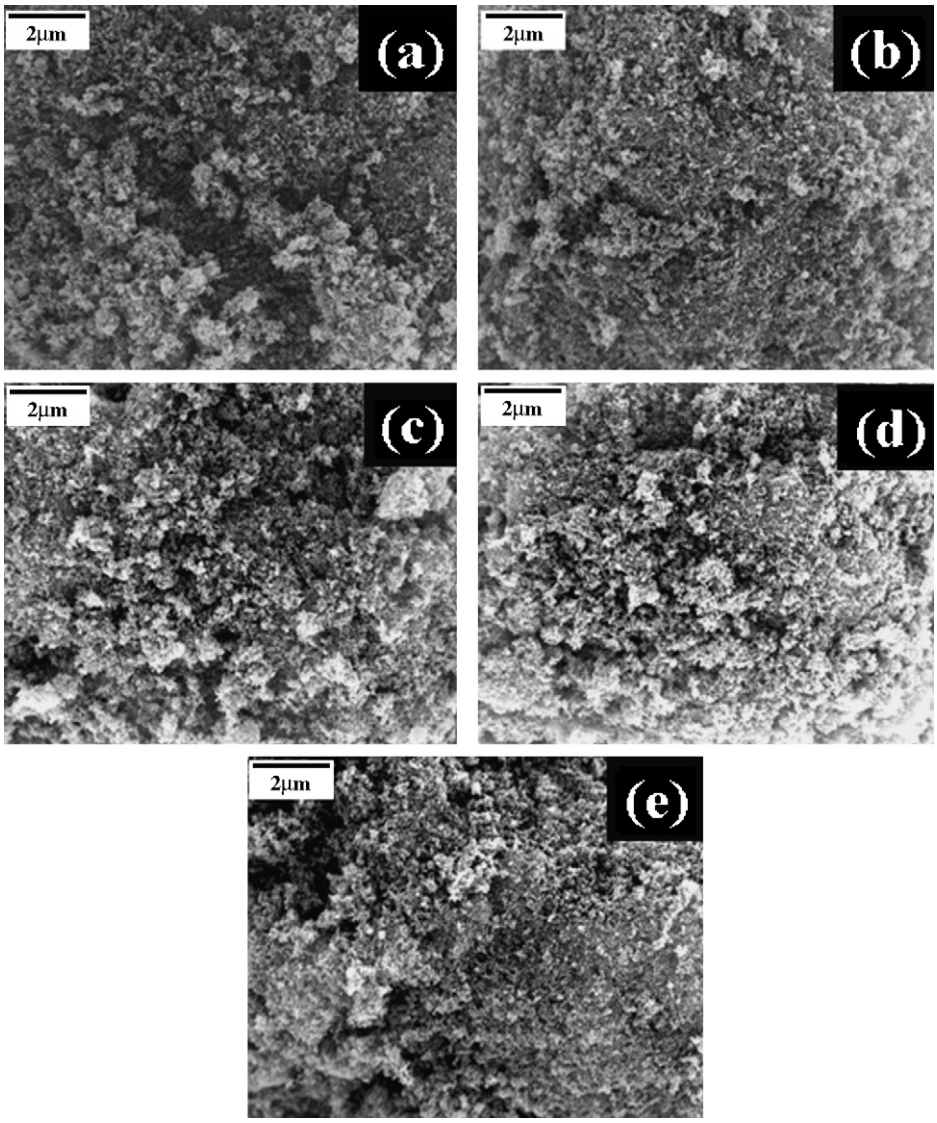

Fig. 2. Scanning electron microscopic images of carbon-supported Pt and Pt–Co catalysts: (a) Pt/C, (b) Pt–Co(4:1)/C, (c) Pt–Co(3:1)/C, (d) Pt–Co(2:1)/C, and (e) Pt–Co(1:1)/C.

3.3. Electrochemical active surface area (EAS) of the catalysts

Cyclic voltammetry was employed to calculate the electrochemical active area of the carbon-supported Pt and Pt_xCo_y catalysts [23]. The cyclic voltammograms obtained on the prepared catalysts with a CO adsorbed ad-layer in the potential region of +0.5 and +1.1 V vs. NHE are shown in Fig. 3. The peak at about 0.87 V vs. NHE represents the electrooxidation of the irreversibly adsorbed CO. The electrochemical active surface area (EAS) is calculated using the formula: EAS = Q_{CO}/(Pt loading × 0.484) where Q_{CO} is the overall CO_{ads} stripping charge and 0.484 is the charge required to oxidize a monolayer of CO on polycrystalline Pt [28]. The calculated EAS values are given in Table 1. It is calculated to be 65.2, 51.4, 47.7, 41.5 and 38.3 $m^2\,g^{-1}$ Pt (within the error limits of ±5) for Pt/C, Pt–Co(4:1)/C, Pt–Co(3:1)/C, Pt–Co(2:1)/C and Pt–Co(1:1)/C catalysts, respectively.

3.4. Characterization of the polymer

PBI synthesized using polyphosphoric acid process was characterized by means of inherent viscosity (IV) and phosphoric acid content. The acid content of home-made PBI membrane is 85 wt.% which corresponds to 18 mol of phosphoric acid per mol of polymer repeating unit. These results are in good agreement with results published by other authors using similar materials [29–31].

Inherent viscosity, which is an indirect measure of the molecular weight, was in the interval of 0.7–0.9 $dL\,g^{-1}$, depending on the batch. The molecular weight calculated using Mark–Houwink expression [32,33] was in the interval 115,000–150,000 $g\,mol^{-1}$, which corresponds to moderate molecular weight polymer [34].

3.5. Performance and durability of Pt_xCo_y/C cathode materials in HT-PEMFCs

Electrode resistance measured by impedance spectroscopy in H_2/N_2 mode was found to be 1.1 ± 0.3 Ohm-cm^2 at 160 °C. This value is high when compared with commercial Pt/C catalyst (0.1 ohm-cm^2). This is probably due to the semi-metallic nature of the alloying element and contact resistances in the fuel cell.

The fuel cell performance curves, i.e., iR-corrected polarization curves recorded at 160 and 180 °C are shown in Figs. 4 and 5 respectively. The corresponding open circuit voltage (OCV) and electrochemical performances are given in Table 2. Pt–Co alloys exhibited an open circuit voltage of ≥0.9 V at both 160 and 180 °C which is comparable with that found with Pt (~0.9 V). At low current densities (200 $mA\,mg^{-1}$ Pt), Pt–Co alloys (with Co loadings

Table 2
High temperature PEMFC performance of Pt and Pt_xCo_y cathodes.

Catalyst	OCV (V) at 160 °C	Voltage at 200 mA mg^{-1} Pt in PEMFC operated at 160 °C	OCV (V) at 180 °C	Voltage at 200 mA mg^{-1} Pt in PEMFC operated at 180 °C
Pt/C	0.90	0.605	0.87	0.51
Pt–Co(4:1)/C	0.92	0.595	0.91	0.565
Pt–Co(3:1)/C	0.935	0.62	0.93	0.615
Pt–Co(2:1)/C	0.94	0.62	0.935	0.62
Pt–Co(1:1)/C	0.92	0.625	0.915	0.63

of Pt–Co(3:1) and higher) exhibited good performance compared with that of Pt/C. At high current densities (>200 mA mg^{-1} Pt), Pt–Co(1:1)/C and Pt–Co(2:1)/C exhibited good performance with low polarization losses among the investigated catalysts. The improvement in the electrochemical performance of the Pt–Co catalysts with respect to pure Pt is due to the change in the Pt–Pt interatomic distance and surface structure of Pt by the alloying element, Co [5,6,22,35]. Studies performed on Pt–Co bulk alloys [36] also showed that the surface region is dealloyed by oxidation to form a cobalt oxide overlayer when heated in oxygen at

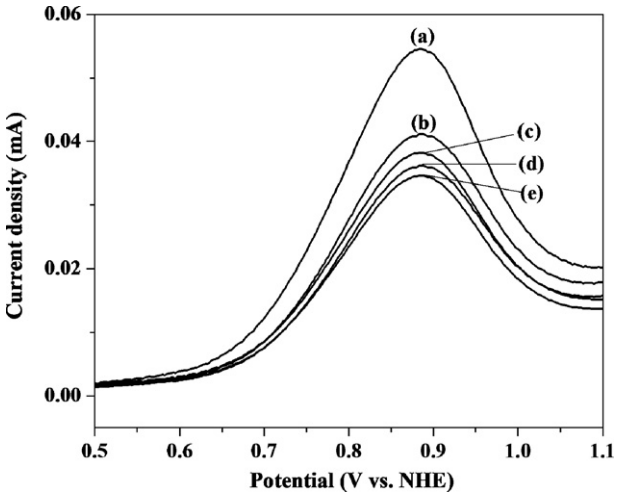

Fig. 3. CO-stripping voltammograms of carbon-supported Pt and Pt–Co catalysts: (a) Pt/C, (b) Pt–Co(4:1)/C, (c) Pt–Co(3:1)/C, (d) Pt–Co(2:1)/C, and (e) Pt–Co(1:1)/C in 0.5 M $HClO_4$ at 10 mV s^{-1}.

fuel cell operating temperatures. The oxide overlayer dissolves in hot concentrated phosphoric acid, leaving a dealloyed pure Pt surface region on top of the bulk alloy. Moreover, XPS data suggested that the amount of platinum oxide content in the carbon-supported Pt–Co alloy electrocatalyst is lower than that in Pt [37], which could explain why the catalysts containing more Co outperform Pt/C catalyst especially at higher temperatures in the highly oxidizing environment encountered in the high temperature PEMFC. Popov and co-workers also reported the good stability of Pt alloys compared to that of pure Pt catalysts under fuel cell conditions [38,39]. They proposed that it might be due to the lower rate of Pt oxidizability, Pt dissolution–redeposition and sintering of Pt alloy particles when compared to pure Pt catalysts under fuel cell conditions. The lower rate of Pt oxidizability (which reflects the stability) in the Pt_xCo_y/C catalysts compared to pure Pt can be explained by the d-orbital coupling between the low occupancy of d-orbitals in Co and high occupancy of d-orbitals in Pt which leads to the decrease of the DOS at the Fermi level of Pt and down shift the Pt d-band center energy [35,40]. The foreign atoms in the Pt_xCo_y alloys behave as electron donors to the Pt atom; thus Pt becomes negatively charged and Co becomes positively charged. As a result, it causes the strong interaction of Co with the negatively charged O of the oxygenated species. The binding energies of several oxygenated species such as O, OH, and H_2O to bimetallic clusters PtCo, PtPtCo and PtCoCo calculated by DFT calculations also show that the second metal element in the alloy has a stronger affinity for OH, O, and H_2O than the Pt sites [40].

The stability of the Pt–Co catalysts in a high temperature fuel cell was tested to prove that the catalyst can be used in realistic applications. Since the degradation of the catalyst occurs at high temperatures, PEM fuel cell was operated at 180 °C and the cell voltage–time plot of the catalysts was recorded for 50 h by

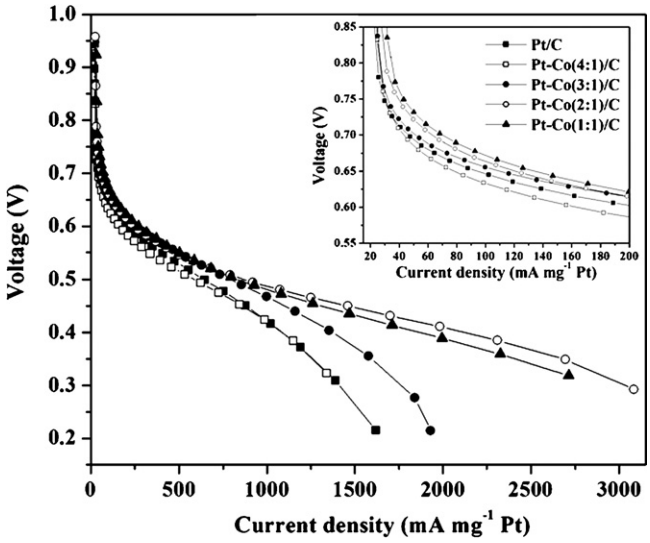

Fig. 4. H_2/O_2 HT-PEMFC polarization curves (iR-corrected) with Pt/C (anode) and Pt_xCo_y/C (cathode) electrocatalysts with various Co contents for oxygen reduction at 160 °C and 1 atm (inset shows the comparison at low current density).

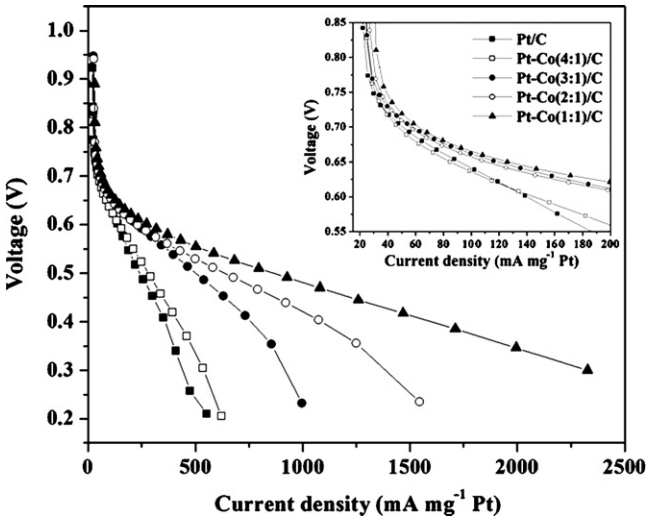

Fig. 5. H_2/O_2 HT-PEMFC polarization curves (iR-corrected) with Pt/C (anode) and Pt_xCo_y/C (cathode) electrocatalysts with various Co contents for oxygen reduction at 180 °C and 1 atm (inset shows the comparison at low current density).

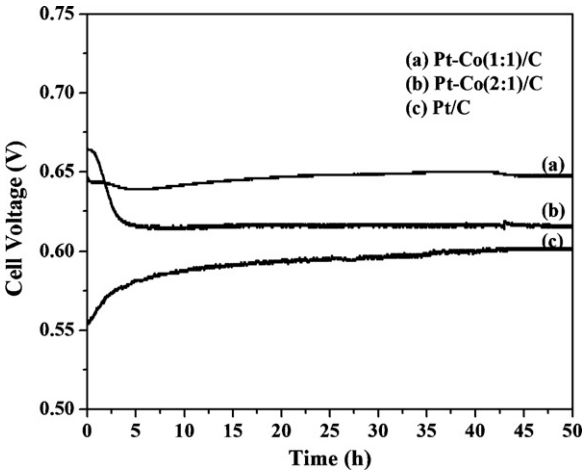

Fig. 6. Cell voltage–time plots of Pt/C and Pt_xCo_y/C electrocatalysts with various Co contents for 50 h of PEMFC operating at 180 °C and 100 mA mg^{-1} Pt.

drawing a constant current of 100 mA mg^{-1} Pt. The corresponding cell voltage–time plot of the catalysts under the identical PEMFC conditions is shown in Fig. 6. It indicates that the Pt–Co(1:1) and Pt–Co(2:1) catalysts were stable at high temperatures (180 °C) under highly oxidizing conditions (cathode at 0.5–0.6 V in presence of pure oxygen). Also the performance is higher than that of Pt/C. Membrane resistance was also stable during the experiment proving the absence of electrolyte loss (phosphoric acid contained in the PBI membrane).

4. Conclusions

Carbon-supported Pt–Co alloy nanoparticles of varying Pt:Co atomic ratios were prepared by borohydride reduction method and characterized using XRD, SEM, EDX, and electrochemical impedance spectroscopy. High temperature PEMFC measurements were performed at 160 and 180 °C using PBI-MEAs based on Pt–Co(1:1 and 2:1) alloys showed good performance. Durability tests performed in a high temperature PEM fuel cell at 180 °C and 100 mA mg^{-1} Pt probed that Pt–Co(1:1 and 2:1) catalysts were stable during 50 h of operation. Membrane resistance was constant during the test proving the absence of phosphoric acid loss. The good performance and stability of the Pt–Co(1:1)/C and Pt–Co(2:1)/C make them as applicable cathodes for high temperature PEMFCs.

Acknowledgements

This work is supported by U.S.-DOD-ARO under the grant # W911NF-08-C-0415 and W911NF-07-1-0426. RB and his scholars (Ch. V. Rao, Javier Parrondo, and Mrs. S.Ghatty) thank Dr. Robert Mantz (Electrochemistry and Advanced Energy Conversion) at ARO-Chemical Sciences, and Dr.Thomas L. Reitz (Electrochemistry and Thermal Sciences at AFRL, Wright Patterson Airbase, OH) for supporting fuel cell research at SUBR.

References

[1] J. Zhang, Z. Xie, J. Zhang, Y. Tang, C. Song, T. Navessin, Z. Shi, D. Song, H. Wang, D.P. Wilkinson, Z.-S. Liu, S. Holdcroft, J. Power Sources 160 (2006) 872.
[2] C. Lamy, A. Lima, V. Lerhun, F. Delime, C. Coutanceau, J.M. Léger, J. Power Sources 105 (2002) 105.
[3] T.R. Ralph, M.P. Hogarth, Platinum Met. Rev. 46 (2002) 3.
[4] H.A. Gasteiger, S.K. Shyam, B. Sompalli, F.T. Wagner, Appl. Catal. B: Environ. 56 (2005) 9.
[5] S. Mukerjee, S. Srinivasan, J. Electroanal. Chem. 357 (1993) 201.
[6] S. Mukerjee, S. Srinivasan, M.P. Soriaga, J. McBreen, J. Phys. Chem. 99 (1995) 4577.
[7] T. Toda, H. Igarashi, H. Uchida, M. Watanabe, J. Electrochem. Soc. 146 (1999) 3750.
[8] U.A. Paulus, A. Wokaun, G.G. Scherer, T.J. Schmidt, V. Stamenkovic, V. Radmilovic, N.M. Markovic, P.N. Ross, J. Phys. Chem. B 106 (2002) 4181.
[9] L. Xiong, A.M. Kannan, A. Manthiram, Electrochem. Commun. 4 (2002) 898.
[10] E. Antolini, J.R.C. Salgado, E.R. Gonzalez, J. Power Sources 160 (2006) 957.
[11] A.K. Shukla, R.K. Raman, N.A. Choudhury, K.R. Priolkar, P.R. Sarode, S. Emura, R. Kumashiro, J. Electroanal. Chem. 563 (2004) 181.
[12] H. Yang, W. Vogel, C. Lamy, N. Alonso-Vante, J. Phys. Chem. B 108 (2004) 11024.
[13] H. Yang, N. Alonso-Vante, J.-M. Lèger, C. Lamy, J. Phys. Chem. B 108 (2004) 1938.
[14] W. Li, W. Zhou, H. Li, Z. Zhou, B. Zhou, G. Sun, Q. Xin, Electrochim. Acta 49 (2004) 1045.
[15] E. Antolini, J.R.C. Salgado, L.G.R.A. Santos, G. Garcia, E.A. Ticianelli, E. Pastor, E.R. Gonzalez, J. Appl. Electrochem. 36 (2006) 355.
[16] T. Ioroi, K. Yasuda, J. Electrochem. Soc. 152 (2005) A1917.
[17] A. Sode, W. Li, Y. Yang, P.C. Wong, E. Gyenge, K.A.R. Mitchell, D. Bizzotto, J. Phys. Chem. B 110 (2006) 8715.
[18] Q. Huang, H. Yang, Y. Tang, T. Lu, D.L. Akins, Electrochem. Commun. 8 (2006) 220.
[19] V.A. Rinberg, T.L. Kulova, N.A. Maiorova, Zh.V. Dobrokhotova, A.A. Pasynskii, A.M. Skundin, O.A. Khazova, Russ. J. Electrochem. 43 (2007) 75.
[20] H. Li, G. Sun, N. Li, S. Sun, D. Su, Q. Xin, J. Phys. Chem. C 111 (2007) 5605.
[21] Y. Qian, W. Wen, P.A. Adcock, Z. Jiang, N. Hakim, N. Saha, S. Mukerjee, J. Phys. Chem. C 112 (2008) 1146.
[22] V. Jalan, E.J. Taylor, J. Electrochem. Soc. 130 (1983) 2299.
[23] A. Pozio, M. De Francesco, A. Cemmi, F. Cardellini, L. Giorgi, J. Power Sources 105 (2002) 13.
[24] L. Xiao, H. Zhang, T. Jana, E. Scanlon, R. Chen, E.W. Choe, L.S. Ramanathan, S. Yu, B.C. Benicewicz, Fuel Cells 5 (2005) 287.
[25] J. Mader, L. Xiao, T.J. Schmidt, B.C. Benicewicz, Adv. Polym. Sci. 216 (2008) 63.
[26] M.C. Lefebvre, R.B. Martin, P.G. Pickup, Electrochem. Solid-State Lett. 2 (1999) 259.
[27] Y. Liu, M. Murphy, D.R. Baker, W. Gu, C. Ji, J. Jorne, H.A. Gasteiger, Proton Exchange Membrane Fuel Cells 7, vol. 11, The Electrochemical Society Inc., Pennington, 2007, p. 473.
[28] M. Ciureanu, H. Wang, J. Electrochem. Soc. 146 (1999) 4031.
[29] T.J. Schmidt, J. Baurmeister, ECS Trans. 16 (2008) 263.
[30] T.J. Schmidt, ECS Trans. 1 (2006) 19.
[31] T.J. Schmidt, J. Baurmeister, J. Power Sources 176 (2008) 428.
[32] E.W. Choe, US Patent US4312976 (1982).
[33] E.W. Choe, A.B. Conciatori, US Patent US4535144 (1985).
[34] J.S. Wainright, J.T. Wang, D. Weng, R.F. Savinell, M. Litt, J. Electrochem. Soc. 142 (1995) L121.
[35] Ch. Venkateswara Rao, B. Viswanathan, J. Phys. Chem. C 113 (2009) 18907.
[36] U. Bardi, B. Beard, P.N. Ross, J. Vasc. Sci. Technol. A 6 (1988) 665.
[37] A.K. Shukla, M. Neergat, P. Bera, V. Jayaram, M.S. Hegde, J. Electroanal. Chem. 504 (2001) 111.
[38] H.R. Colon-Mercado, B.N. Popov, J. Power Sources 155 (2006) 253.
[39] H.R. Colon-Mercado, H. Kim, BN. Popov, Electrochem. Commun. 6 (2004) 795.
[40] P.B. Balbuena, D. Altomare, N. Vadlamani, S. Bingi, L.A. Agapito, J.M. Seminario, J. Phys. Chem. B 108 (2004) 6378.